ENGINEERING

Instability mediated self-templating of drop crystals

Lingzhi Cai[1], Joel Marthelot[1,2], P.-T. Brun[1]*

The breakup of liquid threads into droplets is prevalent in engineering and natural settings. While drop formation in these systems has a long-standing history, existing studies typically consider axisymmetric systems. Conversely, the physics at play when multiple threads are involved and the interaction of a thread with a symmetry breaking boundary remain unexplored. Here, we show that the breakup of closely spaced liquid threads sequentially printed in an immiscible bath locks into crystal-like lattices of droplets. We rationalize the hydrodynamics at the origin of this previously unknown phenomenon. We leverage this knowledge to tune the lattice pattern via the control of injection flow rate and nozzle translation speed, thereby overcoming the limitations in structural versatility typically seen in existing fluid manipulations paradigms. We further demonstrate that these drop crystals have the ability to self-correct and propose a simple mechanism to describe the convergence toward a uniform pattern of drops.

INTRODUCTION

In the Rayleigh-Plateau instability of a flowing jet, interfacial perturbations can be modeled as exponential functions with complex frequencies and wavelengths whose superposition generates wave packets that travel both upstream and downstream until the thread breaks to generate drops (*1*–*4*). Depending on the setting, these droplets are the vehicle for biological material, drugs, and polymeric solutions or are destined to combustion, while their radius may range anywhere from a few millimeters to tens of nanometers (*5*–*10*). In addition to its applicability, the breakup of jets illustrates key phenomena in the physics of fluids, e.g., absolute/convective instabilities and singularities. Hence, the Rayleigh-Plateau instability has been extensively studied, albeit primarily in the context of a single jet and assuming axisymmetry (*4*). Therefore, little is known on the collective stability of multiple threads (*11*–*13*); in particular, the case of the successive breakups of neighboring jets has never been reported. Here, we show that viscous threads sequentially extruded into another immiscible viscous bath lead to the self-assembly of complex droplet lattices. This self-templating effect is underpinned by the noise amplifier nature of the instability that turns the infinitesimal perturbations of the interface of a thread into drops (*14*, *15*). Here, perturbations in a given thread are inherited from breakup events in previously extruded threads, thereby slowly building up memory in the system that eventually converges toward a crystalline structure. With our technique, the size of droplets and their arrangements are fully controlled by fluid dynamics. While packed hexagonal lattices are routinely used in top-down fabrication methods (*16*–*19*), the flexibility of our approach allows for the assembly of previously impossible complex arrays, which can subsequently be polymerized as a route to design functional materials (*20*–*24*). More generally, these droplet assemblies could find widespread application in many fields, including microbiology (*25*–*27*), tissue engineering (*28*), acoustics (*29*, *30*), optics (*31*, *32*), and electrical components (*33*, *34*).

RESULTS

In Fig. 1A, we show our printing system where glycerol is injected through a moving nozzle into an immiscible silicone oil bath to form a liquid jet. The jet follows the trajectory of the nozzle before it breaks into droplets. Here, we show that the printing process builds on the hydrodynamical interaction of a thread with the surrounding environment (Fig. 1B). In particular, the sequential deposition and breakup process gives rise to a crystal-like lattice of droplets, as evident in Fig. 1C (see movie S1). As evident from the Voronoi diagram overlaid on the figure, the array gets more uniform as more rows are added and the defects present in the first lines are progressively smoothed out.

To elucidate the physics at play in our problem, we develop model experiments involving solid templates designed to emulate the presence of nearby droplets. In Fig. 2A, we show a photograph of an experiment where a liquid jet is breaking up near a solid template, with wavelength λ* matching that of the Rayleigh-Plateau instability (see movie S2) (*35*). The value of λ* scales with the radius of the injected jet, h_0, in turn, determined by mass conservation, $h_0 = \sqrt{Q/(\pi U_0)}$, where Q is the injection flow rate and U_0 is the speed of the nozzle (*10*). Geometry is anticipated to matter here, i.e., the

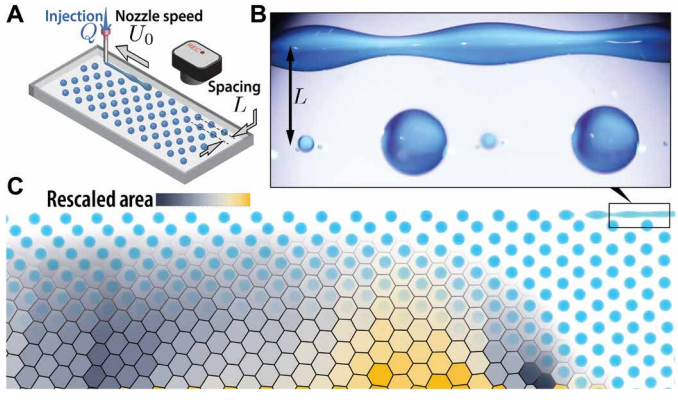

Fig. 1. Sequential breakup of viscous threads. (**A**) Schematic of the experimental setup: Glycerol is injected from a nozzle into a reservoir of silicone oil. A jet develops at the nozzle outlet and breaks up into droplets because of the Rayleigh-Plateau instability. (**B**) Close-up photograph showing the developing troughs and peaks along the jet next to the adjacent droplets. (**C**) Snapshot of the printing experiment with the nozzle speed U_0 = 4.7 mm/s, flow rate Q = 0.21 ml/min, and spacing L = 3.0 mm. The rows are printed in alternating directions, and the drops progressively arrange into an ordered lattice. Overlaid is the Voronoi tessellation obtained from the drop centroids and color coded using the relative area of each cell.

[1]Department of Chemical and Biological Engineering, Princeton University, Princeton, NJ 08540, USA. [2]Aix-Marseille University, CNRS, IUSTI, 13013 Marseille, France. *Corresponding author. Email: pbrun@princeton.edu

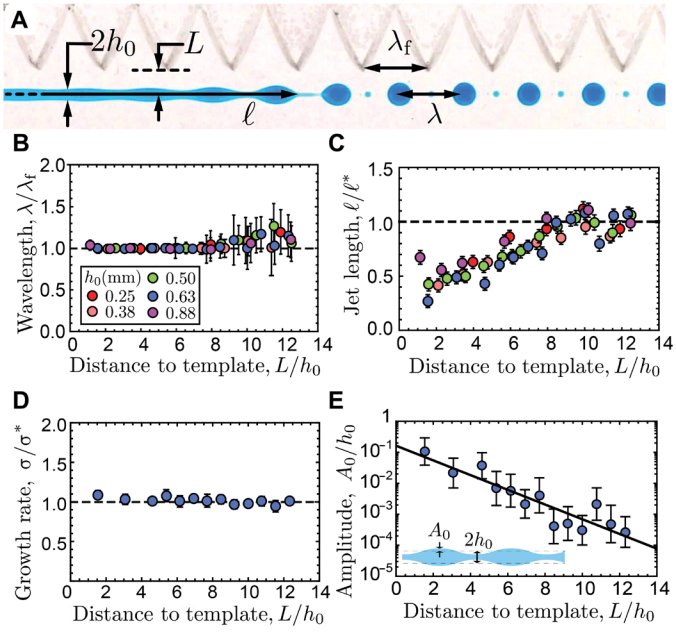

Fig. 2. Enforcing a wavelength. (**A**) Photograph of an experiment of a jet with radius h_0 printed at a distance L of an acrylic template (top view). (**B**) Breakup wavelength λ and (**C**) jet length ℓ as a function of normalized distance to template L for different radius of injected jet h_0. (**D**) Growth rate σ as a function of normalized distance to template L. Dashed lines are the prediction from linear stability analysis. (**E**) Initial perturbation A_0/h_0 as a function of normalized distance to template L. The solid line is the best fit to the experimental data.

relative magnitude of the distance to template L and h_0. In particular, in Fig. 2B, we show that when L decreases, the SD in the observed breakup wavelength λ decreases too, as indicated by the size of error bars. We also find that with $L/h_0 \leq 8$, the SD in wavelength is consistently low. These results suggest that the jet radius h_0 is the relevant length scale in this problem. This point is further confirmed by examining the length of the jet, ℓ, defined as the distance from the nozzle to the point where droplets are shedding. As evident from Fig. 2C, ℓ increases with L/h_0 until it reaches the limiting value ℓ^* of the unbounded case for $L/h_0 \sim 8$ (*10*). To further quantify the role of the template and elucidate the mechanism at play, we measure the growth of the periodic perturbations leading to the jet breakup and compare the results to that of linear stability analysis, where the jet radius is assumed to be $h(x, t) = h_0 + A_0 e^{\sigma t} \cos kx$ (*3*, *4*, *36*). In Fig. 2D, we show that the observed growth rate σ is constant and independent of L. Therefore, the template does not affect the instability intrinsically. Rather, the template alters the initial conditions of the problem in the form of A_0. A_0 is indirectly measured using the jet length data (see Materials and Methods). In Fig. 2E, we show that A_0 decreases exponentially as L increases. Close enough from the template, the jet is, thus, seeded with deformations substantially larger than the ambient noise and whose wavelength follows that of the template. Hence, the breakup pattern locks with the template, thereby improving the droplet monodispersity.

With our solid templates, we also demonstrate the possibility of enforcing wavelengths that deviate from the natural breakup wavelength λ*. In Fig. 3A, typical breakup patterns with different template wavelengths λ_f are shown. As evident from the figure, the distance between drops is a complex function of that of the template. In particular,

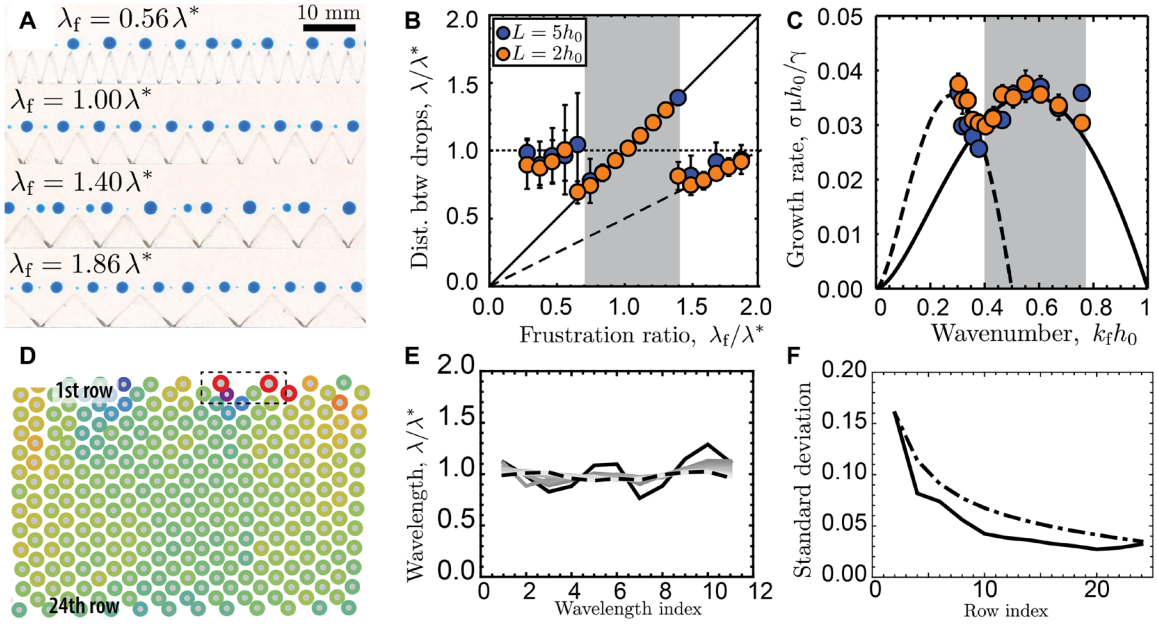

Fig. 3. Tuning the wavelength. (**A**) Photographs of jet breakup with initial radius $h_0 = 0.63$ mm and templates with different forcing wavelength λ_f ($L = 2h_0$). (**B**) Distance between the biggest drops λ/λ^* versus the frustration ratio λ_f/λ^*, with $L = 5h_0$ and $2h_0$. The error bars correspond to the SD of measurements. The gray band indicates the range of enforced wavelengths as determined experimentally. This range is reported in (**C**) where the corresponding growth rates are shown. The solid and dashed curves are the linear dispersion relations for the fundamental harmonic and superharmonic regimes, respectively. (**D**) Self-correcting of wavelengths starting from a polydispersed row. The lattice pattern becomes more regular as rows are printed. (**E**) The observed evolution of the wavelengths across the rows in (D). The 2nd and the 24th rows are shown by the solid and dotted lines, respectively. (**F**) Comparison of SD in wavelength between the observed evolution (solid line) and the model prediction (dash-dotted line).

we observe locking in the range $0.7\lambda^* < \lambda_f < 1.4\lambda^*$, as detailed next. When $\lambda_f < 0.7\lambda^*$, the resulting breakup pattern is highly irregular with negligible locking effect, and the observed mean breakup wavelength remains close to λ^* (shown in Fig. 3B). In the range $0.7\lambda^* < \lambda_f < 1.4\lambda^*$, the breakup wavelength λ follows λ_f closely. A much lower degree of polydispersity than that observed in unbounded breakups is observed, consistent with the aforementioned case $\lambda_f = \lambda^*$. The corresponding growth rate follows the prediction from linear stability analysis (*35*), which is plotted as the black curve in Fig. 3C. We also note that the satellite drops, i.e., the small drops in between, become larger as λ_f increases. When close to the transitional value $\lambda_f \sim 1.4\lambda^*$, we observed unstable breakups yielding drops of varying sizes between the main drops (see fig. S1). As λ_f is further increased, $\lambda_f > 1.4\lambda^*$, the breakup pattern becomes stable again, producing two large drops per forcing wavelength. In this superharmonic regime, the observed wavelength is half that of the forcing (*37*). The dispersion relation for this superharmonic regime is plotted as the dashed curve in Fig. 3C and intersects the fundamental harmonic dispersion at $k_f h_0 = 0.37$, which gives a transition threshold ratio at $\lambda_f/\lambda^* = 1.51$. This value is close to the transition observed experimentally as shown in Fig. 3 (B and C). These results further confirm that the mechanism behind the wavelength locking effect is primarily underpinned by a modification of the initial conditions of the problem by the template. The remainder of the dynamics, e.g., the dispersion relation of the instability, appears to be unaffected by the template.

After describing the effects of a solid template, we now demonstrate that droplets themselves can serve as templates. When printing a thread next to a row of droplets with a well-defined wavelength, we find that the breakup pattern follows the same wavelength (see movie S2). Hence, printing multiple lines parallel to a template leads to the emergence of a regular lattice of drops (see fig. S2). In addition, we have found that similar types of ordered droplet arrays also emerge when starting from a row whose breakup pattern is irregular, i.e., a self-templating effect. In Fig. 3D, we show a typical droplet pattern observed when sequentially printing parallel threads without a solid template. The first row is unbounded and presents some polydispersity (*10*, *38*). As more rows are printed, the breakup progressively corrects itself such that a regular crystal-like pattern eventually emerges. In Fig. 3D, we circle the drops with color coding for their size. In particular, the distance between the two large drops in the first row (highlighted in the dotted box) is $\lambda \simeq 1.70\lambda^*$. In the next row, one wavelength is inserted such that the distance between drops is $\lambda = 0.95\lambda^*$. This observation is consistent with our previous discussion on the competition between harmonic modes. In this case, the smaller wavelengths are closer to the optimal value and, thus, grow faster than the large wavelength. From the second row onward, there is no marked change in the number of drops and, thus, wavelength, but a subtle converging process continues. The rescaled wavelengths in every other row are shown in Fig. 3E. As evident from the figure, the initial nonuniformity in the pattern is progressively smoothed. We find that the convergence toward a lattice structure is iterative in nature and can be captured by a moving average model (see Materials and Methods and Fig. 3F). Any randomly distributed noise oscillating around a constant, here, λ^*, therefore eventually vanish, as evident from Fig. 3 (D to F). Likewise, the system also corrects localized defects, e.g., the intentionally seeded defects discussed in the Supplementary Materials. In any case, a regular drop lattice is obtained regardless of the type of initial defect present.

We now turn to study the phase relationship between rows. An out-of-phase relation is typically observed in the simultaneous

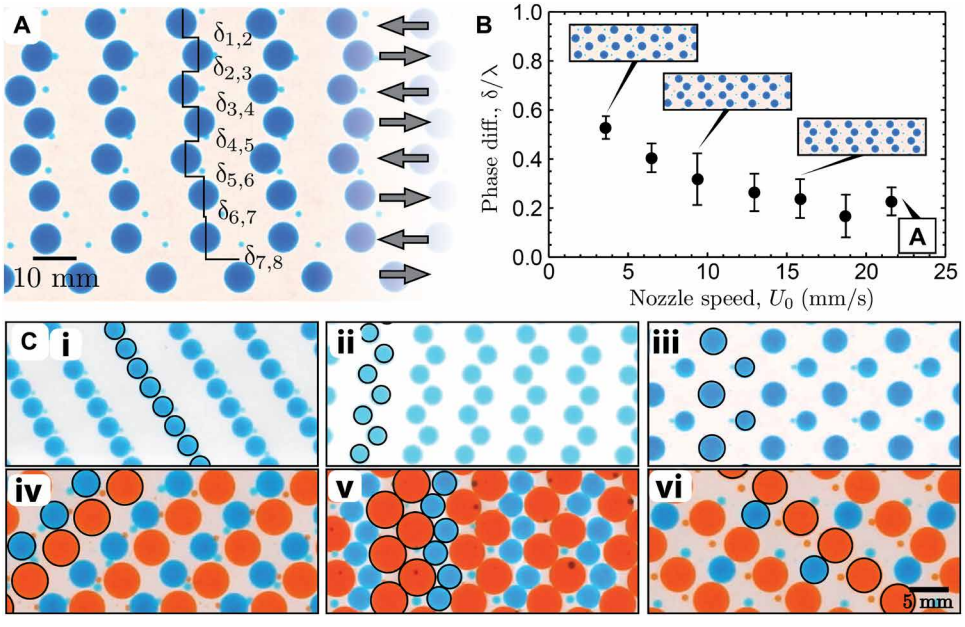

Fig. 4. Designing complex patterns. (**A**) Photograph of a crystal highlighting the phase difference between the drops in adjacent rows. Arrows indicate the nozzle printing direction. (**B**) Final phase difference δ plotted as a function of nozzle speed U_0. The drop radius and the separation between the rows are kept constant, $R = 3.5$ mm and $L = 6.7$ mm. The printing direction is reversed across the neighboring rows, as shown in (A). (**C**) Drop patterns printed (i) $U_0 = 7.2$ mm/s, $Q = 0.25$ ml/min, $L = 1.7$ mm; (ii) $U_0 = 56.9$ mm/s, $Q = 1.98$ ml/min, $L = 1.7$ mm; and (iii) $U_0 = 3.9$ and 7.2 mm/s, $Q = 0.25$ ml/min, $L = 2.4$ mm. In (iv) to (vi), orange droplets are printed first ($U_0 = 10.8$ mm/s, $Q = 0.97$ ml/min, $L = 2.0$ mm), followed by blue droplets ($U_0 = 10.8$ mm/s, $Q = 0.47$ ml/min, $L = 2.0$ or 4.0 mm). Printing direction is as follows: (i), (iv), and (vi) are unidirectional and (ii), (iii), and (v) are alternating.

breakup of multiple liquid threads (*11*, *13*, *39*–*41*). In contrast, our technique generates different phase relations as the lattice is the result of a dynamic process. The drops are dragged long after they are formed when printing subsequent rows (see movie S3). In Fig. 4A, we show the phase difference $\delta_{i,i+1}$, between consecutive lines i and $i+1$. These quantities evolve each time a line is added, e.g., $\delta_{7,8}(t+\Delta t) = \delta_{6,7}(t)$, owing to the periodic nature of the problem. Eventually, these values converge to the final phase difference δ, thus depending on the initial phase difference and successive shifts (see Supplementary Note and figs. S5 to S7). Hence, we are able to tune this quantity $0.2 \leq \delta/\lambda \leq 0.5$ by merely modifying the nozzle speed U_0 (see Fig. 4B for zigzag printing patterns). Likewise, the relative printing direction between rows affects the overall pattern. In Fig. 4C, we show that a variety of drop crystals can be produced by adjusting the injection flow rate, adjusting the nozzle translation speed, or changing the printing direction in different rows (Fig. 4C, i and ii). In addition, we leverage our understanding of the problem to produce complex patterns, e.g., with two populations of monodisperse drops (Fig. 4C, iv to vi). To obtain these structures, we print jets with different thread radii, h_1 and $h_2 \simeq 0.5h_1$ (shown as orange and blue, respectively). Stability analysis predicts that the natural breakup of these individual threads would yield wavelengths differing by a factor 2, $\lambda_2 \simeq 0.5\lambda_1$. In stark contrast, we manage to force these wavelengths to be equal by templating (see movie S4). First, the threads with radius h_1 are printed next to a solid template with wavelength $\lambda_f \simeq 0.7\lambda_1$ and yield a first set of drops (orange in the figure). This forcing matches the left boundary of the templating regime shown in Fig. 3B. Second, the threads with radius h_2 are printed just atop the already formed droplets. These droplets with wavelength λ_f now serve as templates for the breakup of the newly printed threads $\lambda_f \simeq 1.4\lambda_2$ (the right boundary of the templating domain in Fig. 3B). Because glycerol is denser than the surrounding oil, the blue droplets sink in between the orange ones. Using the same protocol, but changing the relative printing directions and interthread gap, offers ways to tune the geometry of the final pattern, as shown in Fig. 4C (iv to vi).

DISCUSSION

In closing, we note that our methodology can be applied to a broad range of fluids so long as jetting is possible (*10*). Hence, our approach is particularly suited to viscous liquids and polymer melts that cannot be handled by microfluidic devices and inkjet printers (*42*) but are necessary to materials science and many industrial applications (*43*). Therefore, our methodology offers a new route for the fabrication of architected materials in a controllable and scalable manner. We envision the freedom in designing the pattern and its flexibility to be adapted to the existing droplet-based technologies that will open up new opportunities as a tool of additive manufacturing.

MATERIALS AND METHODS

Printing setup

Glycerol (99%; Avatar Corporation) is injected through a nozzle with inner radius $r = 0.85$ mm into a reservoir fluid of silicone oil (DMS-T31, Gelest). The fluids have the same viscosity $\mu = 1.1$ Pa·s and the interfacial tension between the fluids is $\gamma = 0.028$ N/m. The flow rate, Q, is imposed using a syringe pump (Chemyx OEM), and we operate in the range $0.25 < Q$ (ml/min) < 4.41, such that the average injection speed at the nozzle is $1.8 < U_i = Q/\pi r^2$ (mm/s) < 32.4. The nozzle is translated in the xy plane using a two-axis translational stage (AxiDraw V3.0) at speed $7.2 < U_0$ (mm/s) < 50.4. The trajectory of the injector is controlled via a software (Inkscape).

Growth of perturbations on liquid threads

The initial stages of breakup are governed by linear theory (*2*, *4*), such that the amplitude of perturbations on the thread grows exponentially. The growth rate σ can thus be estimated from an exponential fit to the temporal evolution of thread radius (*38*, *44*).

We record the breakup of liquid threads at a different distance L away from the solid template. The snapshots of the breakup evolution are binarized. The changes in grayscale at the thread center are measured over time to infer the change in light intensity and, hence, the growth of the amplitude of the perturbations on the thread, according to the Beer-Lambert law. The growth rate σ can then be extracted from the evolution of the growing amplitude.

The initial amplitude of perturbations, A_0, is usually small (less than 1 to 2% of the initial radius h_0) and cannot be measured accurately (*44*). We estimate the ratio A_0/h_0 using the experimental measurements of jet length ℓ and growth rate σ

$$\frac{A_0}{h_0} = e^{-\sigma t_b} = e^{-\sigma \ell / U_0} \tag{1}$$

Here, t_b is the time needed to break the jet, which is given by the intact jet length divided by the nozzle speed U_0 (*4*, *10*).

Moving average model

The converging process is akin to the dilution of variation or frustration in the system by a moving average kernel. In particular, with the kernel $\left(\frac{1}{2}, \frac{1}{2}\right)$, the wavelengths in the later row are given by the average of the two closest neighboring wavelengths in the prior row. The process will repeat for the subsequent rows, resulting in increasingly more uniform breakup patterns (see Supplementary Note and fig. S3). This model can be generalized to other kernels of the form $\left(\frac{1}{a}, \frac{a-1}{a}\right)$ with similar results.

SUPPLEMENTARY MATERIALS

Supplementary material for this article is available at https://science.org/doi/10.1126/sciadv.abq0828

REFERENCES AND NOTES

1. J. Plateau, *Statique expérimentale et théorique des liquides soumis aux seules forces moléculaires*, vol. 2 (Gauthier-Villars, 1873).
2. L. Rayleigh, On the instability of jets. *Proc. Lond. Math. Soc.* **s1-10**, 4–13 (1878).
3. S. Tomotika, On the instability of a cylindrical thread of a viscous liquid surrounded by another viscous fluid. *Proc. R. Soc. Lond. A Math. Phys. Sci.* **150**, 322–337 (1935).
4. J. Eggers, E. Villermaux, Physics of liquid jets. *Rep. Prog. Phys.* **71**, 036601 (2008).
5. R. Seemann, M. Brinkmann, T. Pfohl, S. Herminghaus, Droplet based microfluidics. *Rep. Prog. Phys.* **75**, 016601 (2012).
6. J. J. Kaufman, G. Tao, S. Shabahang, E.-H. Banaei, D. S. Deng, X. Liang, S. G. Johnson, Y. Fink, A. F. Abouraddy, Structured spheres generated by an in-fibre fluid instability. *Nature* **487**, 463–467 (2012).
7. J. Zhang, R. J. Coulston, S. T. Jones, J. Geng, O. A. Scherman, C. Abell, One-step fabrication of supramolecular microcapsules from Microfluidic droplets. *Science* **335**, 690–694 (2012).
8. B. G. Chung, K.-H. Lee, A. Khademhosseini, S.-H. Lee, Microfluidic fabrication of microengineered hydrogels and their application in tissue engineering. *Lab Chip* **12**, 45–59 (2012).
9. A. Fernandez-Nieves, A. M. Puertas, *Fluids, Colloids and Soft Materials: An Introduction to Soft Matter Physics* (John Wiley & Sons, 2016).
10. L. Cai, J. Marthelot, P.-T. Brun, An unbounded approach to microfluidics using the Rayleigh–Plateau instability of viscous threads directly drawn in a bath. *Proc. Natl. Acad. Sci. U.S.A.* **116**, 22966–22971 (2019).

11. P. Elemans, J. Van Wunnik, R. Van Dam, Development of morphology in blends of immiscible polymers. *AIChE J.* **43**, 1649–1651 (1997).
12. Y. M. Knops, J. J. Slot, P. H. Elemans, M. J. Bulters, Simultaneous breakup of multiple viscous threads surrounded by viscous liquid. *AIChE J.* **47**, 1740–1745 (2001).
13. P. J. Janssen, H. Meijer, P. Anderson, Stability and breakup of confined threads. *Phys. Fluids* **24**, 012102 (2012).
14. M. Fermigier, L. Limat, J. Wesfreid, P. Boudinet, C. Quilliet, Two-dimensional patterns in Rayleigh-Taylor instability of a thin layer. *J. Fluid Mech.* **236**, 349–383 (1992).
15. J. Marthelot, E. Strong, P. M. Reis, P.-T. Brun, Designing soft materials with interfacial instabilities in liquid films. *Nat. Commun.* **9**, 4477 (2018).
16. Y. A. Vlasov, X.-Z. Bo, J. C. Sturm, D. J. Norris, On-chip natural assembly of silicon photonic bandgap crystals. *Nature* **414**, 289–293 (2001).
17. B. A. Grzybowski, C. E. Wilmer, J. Kim, K. P. Browne, K. J. Bishop, Self-assembly: From crystals to cells. *Soft Matter* **5**, 1110–1128 (2009).
18. A. G. Marin, H. Gelderblom, D. Lohse, J. H. Snoeijer, Order-to-disorder transition in ring-shaped colloidal stains. *Phys. Rev. Lett.* **107**, 085502 (2011).
19. M. A. Boles, M. Engel, D. V. Talapin, Self-assembly of colloidal nanocrystals: From intricate structures to functional materials. *Chem. Rev.* **116**, 11220–11289 (2016).
20. G. Widawski, M. Rawiso, B. François, Self-organized honeycomb morphology of star-polymer polystyrene films. *Nature* **369**, 387–389 (1994).
21. H. Yabu, M. Takebayashi, M. Tanaka, M. Shimomura, Superhydrophobic and lipophobic properties of self-organized honeycomb and pincushion structures. *Langmuir* **21**, 3235–3237 (2005).
22. D. Shin, T. Huang, D. Neibloom, M. A. Bevan, J. Frechette, Multifunctional liquid marble compound lenses. *ACS Appl. Mater. Interfaces* **11**, 34478–34486 (2019).
23. G. Villar, A. D. Graham, H. Bayley, A tissue-like printed material. *Science* **340**, 48–52 (2013).
24. H. J. Mea, L. Delgadillo, J. Wan, On-demand modulation of 3D-printed elastomers using programmable droplet inclusions. *Proc. Natl. Acad. Sci. U.S.A.* **117**, 14790–14797 (2020).
25. P. R. Baraniak, T. C. McDevitt, Scaffold-free culture of mesenchymal stem cell spheroids in suspension preserves multilineage potential. *Cell Tissue Res.* **347**, 701–711 (2012).
26. S. Mashaghi, A. Abbaspourrad, D. A. Weitz, A. M. van Oijen, Droplet microuidics: A tool for biology, chemistry and nanotechnology. *Trends Analyt. Chem.* **82**, 118–125 (2016).
27. T. S. Kaminski, O. Scheler, P. Garstecki, Droplet microfluidics for microbiology: Techniques, applications and challenges. *Lab Chip* **16**, 2168–2187 (2016).
28. D. Beattie, K. H. Wong, C. Williams, L. A. Poole-Warren, T. P. Davis, C. Barner-Kowollik, M. H. Stenzel, Honeycomb-structured porous films from polypyrrole-containing block copolymers prepared via raft polymerization as a scaffold for cell growth. *Biomacromolecules* **7**, 1072–1082 (2006).
29. A. Khelif, A. Choujaa, S. Benchabane, B. Djafari-Rouhani, V. Laude, Guiding and bending of acoustic waves in highly confined phononic crystal waveguides. *Appl. Phys. Lett.* **84**, 4400–4402 (2004).
30. R. H. Olsson III, I. El-Kady, Microfabricated phononic crystal devices and applications. *Meas. Sci. Technol.* **20**, 012002 (2009).
31. H. Yabu, M. Shimomura, Simple fabrication of micro lens arrays. *Langmuir* **21**, 1709–1711 (2005).
32. H. Ma, J. Cui, J. Chen, J. Hao, Self-organized polymer nanocomposite inverse opal films with combined optical properties. *Chem. A Eur. J.* **17**, 655–660 (2011).
33. M. A. Holden, D. Needham, H. Bayley, Functional bionetworks from nanoliter water droplets. *J. Am. Chem. Soc.* **129**, 8650–8655 (2007).
34. G. Maglia, A. J. Heron, W. L. Hwang, M. A. Holden, E. Mikhailova, Q. Li, S. Cheley, H. Bayley, Droplet networks with incorporated protein diodes show collective properties. *Nat. Nanotechnol.* **4**, 437–440 (2009).
35. H. Stone, M. Brenner, Note on the capillary thread instability for fluids of equal viscosities. *J. Fluid Mech.* **318**, 373 (1996).
36. F. Gallaire, P.-T. Brun, Fluid dynamic instabilities: Theory and application to pattern forming in complex media. *Philos. Trans. R. Soc. A Math. Phys. Eng. Sci.* **375**, 20160155 (2017).
37. G. Lerisson, P. G. Ledda, G. Balestra, F. Gallaire, Instability of a thin viscous film flowing under an inclined substrate: Steady patterns. *J. Fluid Mech.* **898**, 10.1017/jfm.2020.396, (2020).
38. R. J. Donnelly, W. Glaberson, Experiments on the capillary instability of a liquid jet. *Proc. R. Soc. Lond. A Math. Phys. Sci.* **290**, 547–556 (1966).
39. Z. Zhang, G. Hilton, R. Yang, Y. Ding, Capillary rupture of suspended polymer concentric rings. *Soft Matter* **11**, 7264–7269 (2015).
40. V. Mansard, J. M. Mecca, D. L. Dermody, D. Malotky, C. J. Tucker, T. M. Squires, Collective rayleigh-plateau instability: A mimic of droplet breakup in high internal phase emulsion. *Langmuir* **32**, 2549–2555 (2016).
41. Q. Brosseau, P. M. Vlahovska, Streaming from the equator of a drop in an external electric field. *Phys. Rev. Lett.* **119**, 034501 (2017).
42. A. B. Thompson, C. R. Tipton, A. Juel, A. L. Hazel, M. Dowling, Sequential deposition of overlapping droplets to form a liquid line. *J. Fluid Mech.* **761**, 261–281 (2014).
43. H. Du, A. Cont, M. Steinacher, E. Amstad, Fabrication of hexagonal-prismatic granular hydrogel sheets. *Langmuir* **34**, 3459–3466 (2018).
44. E. Goedde, M. Yuen, Experiments on liquid jet instability. *J. Fluid Mech.* **40**, 495–511 (1970).

Acknowledgments

Funding: This work was supported by NSF via grants NSF CAREER (CBET 2042930) and NSF FMRG (CMMI 2037097). **Author contributions:** P.-T.B. and J.M. designed the research. L.C. performed the experiments. All the authors analyzed the data and wrote the manuscript. **Competing interests:** The authors declare that they have no competing interests. **Data and materials availability:** All data needed to evaluate the conclusions in the paper are present in the paper and/or the Supplementary Materials.

Submitted 16 March 2022
Accepted 23 May 2022
Published 6 July 2022
10.1126/sciadv.abq0828